SAR Imaging Using the Sparse Fourier Transform

Xiaqing (Valerie) Yang, Athina P. Petropulu,
Department of Electrical and Computer Engineering
Rutgers, the State University of New Jersey, Piscataway, New Jersey, 08854, USA
{xiaqing.yang, athinap}@rutgers.edu

***Abstract*—In wide-bandwidth high-resolution synthetic aperture radar (SAR), high sampling rates generate big demands for computations and storage. This paper exploits the sparsity of the electromagnetic reflectivity of far-field targets in the range-azimuth domain to propose a sparse Fourier transform (SFT) based ranged doppler (RD) algorithm for SAR imaging. The proposed algorithm ensures the same resolution as the RD algorithm with computational complexity $O(K \log_2 K)$, where K is of the order of the target scene sparsity, while employing only $O(K \log_2 N)$ samples in azimuth direction and $O(K \log_2 N_t)$ in range direction, where N and N_t denote the number of Nyquist sampling points in azimuth and range direction, respectively.**

I. Introduction

Synthetic aperture radar (SAR) imaging is attracting interest due to superior resolution performance, all-weather condition operation, and good interference suppression performance [1], [2], [4], [5]. In SAR, high resolution in both the azimuth and range direction can be obtained by employing the spotlight mode with wideband signals. For example, a 3GHz bandwidth signal can achieve a resolution of 0.05 meters. When Nyquist rate sampling is performed in the spotlight mode with wideband signals, the large amount of sampled data create big storage and computational complexity issues [1], [2].

SAR imaging algorithms can be divided into time-domain and frequency-domain. Time-domain imaging algorithms include the back propagation (BP) algorithm [1], which provides high resolution and wide applicability but with the price of large computational complexity, long imaging time, and poor real-time performance. Frequency-domain imaging algorithms include the range Doppler (RD) algorithm, the chirp scaling algorithm, the polar format algorithm, and the Omega-k algorithm [1], [2]. One advantage of the frequency-domain imaging algorithms is the reduction of computational complexity achieved by replacing two-dimensional manipulation in the time-domain with two one-dimensional manipulations in the frequency domain.

In this paper we consider a SAR system operating is spotlight mode with wideband waveforms. We focus on frequency domain approaches and consider way to further reduce complexity by exploiting the sparsity of targets. In scenarios in which the targets are sparse, compressed sensing (CS) has been proposed for reducing the amount of data that need to be collected, thus reducing the radar operational cost [4], [5], [11]. However, CS based methods for recovery of the target scene involve high computational complexity and are also sensitive to noise [3].

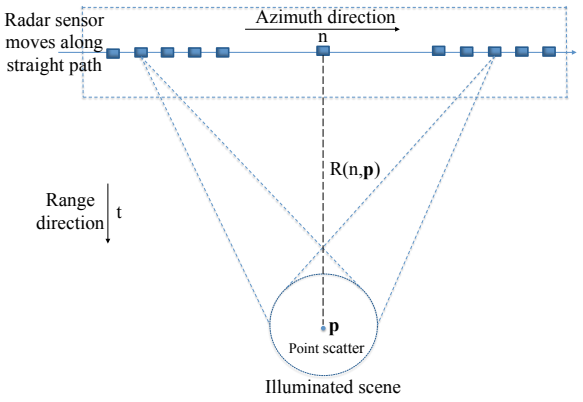

Fig. 1: A brief model of ground-plane geometry for a spotlight mode SAR.

This paper exploits sparsity of targets in the range-azimuth domain in order to reduce the amount of sampling needed. In particular, we follow the RD approach, but forward to the image formation processor (IFP) fewer range and azimuth samples, obtained in a pseudo random fashion. The IFP applies Sparse Fourier Transform (SFT) [7]–[10] in order to perform range and azimuth compression. The number of range samples needed is $O(K \log_2 N_t)$ and the number of azimuth samples needed is $O(K \log_2 N)$, where K is of the order of the target scene sparsity and N, N_t denote the number of Nyquist sampling points in azimuth and range direction, respectively. Typically $O(K \log_2 N_t)$ and $O(K \log_2 N)$ are much smaller than the number of range and azimuth samples N_t and N needed for Nyquist rate sampling. The computational complexity for this SFT based RD algorithm is $O(K \log_2 K)$, which represents a substantial reduction as compared to typical RD approaches, and also CS-based approaches.

The remainder of this paper is organized as follows. Section II presents the general SAR signal model. In Section III, the SAR imaging based on SFT is described in detail. Numerical simulations are provided in Section IV. Finally, Section V concludes this paper.

II. Signal Model of Spotlight Mode SAR

A brief model of ground-plane geometry for a spotlight mode SAR is shown in Fig. 1, where a SAR generates and transmits a sequence of wideband pulses at a constant time interval. In the spotlight mode, the SAR always steers at a

fixed scene as the radar sensor traverses the straight path. The transmitted pulse is of the form

$$f(t) = \exp(j2\pi f_c t)\exp(j\pi\beta t^2)\text{rect}(t), \tag{1}$$

where f_c and β denote the pulse carrier frequency and chirp rate, t is the fast-time variable in range direction and rect(t) equals one in $[-T_c/2, T_c/2]$ and zero elsewhere with T_c denoting the pulse duration.

The demodulated echoes received at the radar sensor with the point scatters located in the illuminated scene Ω can therefore be expressed as

$$\begin{aligned} s(t,n) = &\sum_{\mathbf{p}\in\Omega} \sigma(\mathbf{p}) \exp\left(-j2\pi f_c \frac{2R(n,\mathbf{p})}{c}\right) \\ &\cdot \exp\left(j\pi\beta(t - \frac{2R(n,\mathbf{p})}{c})^2\right) \text{rect}\left(t - \frac{2R(n,\mathbf{p})}{c}\right), \end{aligned} \tag{2}$$

where $\mathbf{p}$ denotes the position of the scatter with corresponding complex reflectivity $\sigma(\mathbf{p})$, n denotes the pulse number and also the slow-time variable in azimuth direction, $R(n,\mathbf{p})$ is the distance between the position of the sensor while transmitting the nth pulse and the position of the scatter $\mathbf{p}$.

III. SAR Imaging using the SFT

A. Imaging Procedures

The classic RD imaging algorithm mainly consists of range compression, range cell migration correction (RCMC) and azimuth compression [1]. When the time delay of receiving the transmitted pulses caused by the location difference of any two scatter in the far-field scene is much smaller than the pulse duration, the *dechirp* technique can be used for range compression [2], [6].

The dechirp in range compression is achieved by multiplying the demodulated received echo (2) with the conjugate of the reference signal,

$$\begin{aligned} s_{RC}(t,n) &= s(t,n)\cdot\exp(-j\pi\beta t^2) \\ &= \sum_{\mathbf{p}\in\Omega} \sigma(\mathbf{p}) A(n,\mathbf{p}) \exp\left(-j2\pi f_c \frac{2R(n,\mathbf{p})}{c}\right) \\ &\cdot \exp\left(-j2\pi\beta t \frac{2R(n,\mathbf{p})}{c}\right) \text{rect}\left(t - \frac{2R(n,\mathbf{p})}{c}\right), \end{aligned} \tag{3}$$

where $A(n,\mathbf{p}) = \exp\left(j\pi\beta(\frac{2R(n,\mathbf{p})}{c})^2\right)$ is known as residual video phase [4]. The term $\exp\left(-j2\pi f_c \frac{2R(n,\mathbf{p})}{c}\right)$ in (3) is the azimuth signal which will be compensated in the azimuth compression step, while the term $\exp\left(-j2\pi\beta t \frac{2R(n,\mathbf{p})}{c}\right)$ in (3) is the range-azimuth coupling term which includes the range cell migration and target range position information. It can be observed that, within the same pulse (the same n), the term $\exp\left(-j2\pi\beta t \frac{2R(n,\mathbf{p})}{c}\right)$ is a complex sinusoid, the frequency of which directly relates to the target position $R(n,\mathbf{p})$. As a consequence, by taking the Fourier transform of (3) with respect to t, the contribution of the scatters in the range direction can be narrowed to the peaks of the spectrum.

However, to eliminate the relevance of different scatters, RCMC is needed before compression. Thus, imaging can therefore be analyzed separately in the range and azimuth direction [1]. Ignoring the spatial variation of the range cell migration, RCMC is implemented by multiplying $s_{RC}(t,n)$ with the reference range migration corrected signal $s_{RCMC}(t)$

$$s_{RCMC}(t) = \exp\left(j2\pi\beta t \frac{2R(n,\mathbf{p}_{ref})}{c}\right), \tag{4}$$

where $\mathbf{p}_{ref}$ denotes the reference target which is always chosen as the center of the illuminated scene $\mathbf{p}_{ref} = \mathbf{0}$. Range compression with RCMC is therefore achieved by

$$\begin{aligned} s_{RCMC}(f_t,n) =& \mathcal{F}_t\{s_{RC}(t,n)s_{RCMC}(t)\} \\ &= \sum_{\mathbf{p}\in\Omega} \sigma(\mathbf{p}) A(n,\mathbf{p}) \exp\left(-j2\pi f_c \frac{2R(n,\mathbf{p})}{c}\right) \\ &\cdot \text{sinc}\left(2\pi(f_t + \beta\frac{2(R(0,\mathbf{p}) - R(0,\mathbf{0}))}{c})\right), \end{aligned} \tag{5}$$

where $R(0,\mathbf{p})$ denotes the initial distance from the SAR platform to the target located at $\mathbf{p}$. When the term $R(0,\mathbf{p}) - R(0,\mathbf{0})$ is equal to zero, it follows that the two scatters $\mathbf{p}$ and $\mathbf{p}_{ref} = \mathbf{0}$ are in the same range bin, while when it is nonzero, the two scatters are not in the same range unit bin.

Next, azimuth compression is needed to focus the exact location of the scatters. Let us assume that in the ℓth ($\ell = 1, 2, ..., N_t$) range bin there are Q_l targets. The received azimuth signal can be expressed as

$$s_{AZI}(n) = \sum_{m=1}^{Q_l} \sigma(\mathbf{p}_m) \exp\left(-j2\pi f_c \frac{2R(n,\mathbf{p}_m)}{c}\right). \tag{6}$$

Under the condition of ignoring the spatial variation of the azimuth signal, the azimuth compression reference signal can be defined as

$$s_{REF}(n) = \exp\left(j2\pi f_c \frac{2R(n,\mathbf{p}_{ref})}{c}\right), \tag{7}$$

where $\mathbf{p}_{ref}$ is always chosen as $\mathbf{p}_0 = \mathbf{0}$. Let us assume that the radar sensor at the initial position $\mathbf{p}_r(0) = [x_0, 0, z_0]$ moves at the speed of $\mathbf{v} = [0, v_y, 0]$ and the targets in the ℓth range bin is located at $\mathbf{p}_m = [x_m, y_m, z_m], m = 1, 2, ..., Q_l$. The received echo in the ℓth range bin after azimuth compression can thus be derived

$$s_{AC}(n) = s_{AZI}(n)s_{REF}(n) \tag{8a}$$

$$= \sum_{m=1}^{Q_l} \sigma(\mathbf{p}_m) \exp\left(-j2\pi f_c \frac{2(R(n,\mathbf{p}_m) - R(n,\mathbf{p}_0))}{c}\right) \tag{8b}$$

$$= \sum_{m=1}^{Q_l} \sigma(\mathbf{p}_m) \exp\left(-j2\pi \frac{2f_c v_y y_m}{cR\cdot\text{PRF}} n\right), n = 0, ..., N-1 \tag{8c}$$

where

$$R = R(n,\mathbf{p}_m) = \sqrt{(x_0 - x_m)^2 + \left(\frac{v_y n}{\text{PRF}} - y_m\right)^2 + (z_0 - z_m)^2},$$

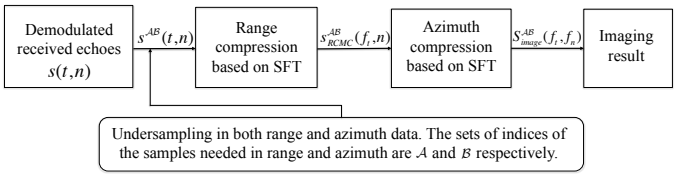

Fig. 2: A block diagram for the SFT based RD algorithm.

$m = 1, 2, ..., Q_l$, since the scatters are assumed in the same range bin and PRF denotes the pulse repetition frequency. (8c) is the linear superposition of Q_l complex sinusoids containing Q_l spatial frequencies, i.e., $\omega_m = \frac{2f_c v_y y_m}{cR \cdot \text{PRF}}$, in which the term y_m is directly related to the scatters locations.

As a consequence, by taking the Fourier transform of (8c) with respect to slow-time n, the contribution of the scatters in the azimuth direction can be narrowed to the peaks of the Doppler spectrum, and this is the azimuth compression can be completed. In the ℓth range bin, the azimuth compressed data is given by

$$\begin{aligned} s_{AC}(f_n) &= \mathcal{F}_n\{s_{AC}(n)\} \\ &= \sum_{m=1}^{Q_l} \sigma(\mathbf{p}_k)\text{sinc}\left(2\pi(f_n + \frac{2f_c v_y y_m}{cR \cdot \text{PRF}})\right), \end{aligned} \tag{9}$$

where $\mathcal{F}_n$ denotes the Fourier transform in the azimuth direction.

Ultimately, after the procedures described above, the output of the imaging result can be represented as

$$\begin{aligned} S_{image}(f_t, f_n) = \sum_{\mathbf{p}\in\Omega} \sigma(\mathbf{p})A(n,\mathbf{p})\text{sinc}\left(2\pi(f_n + \frac{2f_c v_y y_{\mathbf{p}}}{cR \cdot \text{PRF}})\right) \\ \cdot \text{sinc}\left(2\pi(f_t + \beta\frac{2(R(0,\mathbf{p}) - R(0,\mathbf{0}))}{c})\right) \end{aligned} \tag{10}$$

B. Proposed SFT-RD Imaging Algorithm

Based on the previous discussion, range and azimuth compressions can be implemented using Fast Fourier Transforms. The FT peaks after range compression occur at locations directly related to spatial frequencies $R(n, \mathbf{p})$, and the locations of the FT peaks after azimuth compression are directly related to spatial frequencies y_m. However, if the number of scatters Q is much smaller than N and N_t, the image can be sparsely populated in both azimuth and range direction. In such cases, there will be fewer spatial frequencies in (3), (8c) to be determined. The SFT is uniquely suited to identify those frequencies using a small number of samples and involving lower complexity than the FFT. The proposed SFT based RD imaging algorithm is shown in the block diagram of Fig. 2. The locations of the samples needed in range and azimuth directions as included in the sets $\mathcal{A}$ and $\mathcal{B}$ can be calculated as a priori and sent to the radar sensor. Thus, the undersampling of the data can be achieved before the range dechirp procedure.

The SFT algorithm will be applied separately in range and azimuth direction to replace the FFT in (5) and (9). The following discussion is to take the azimuth compression using SFT for instance.

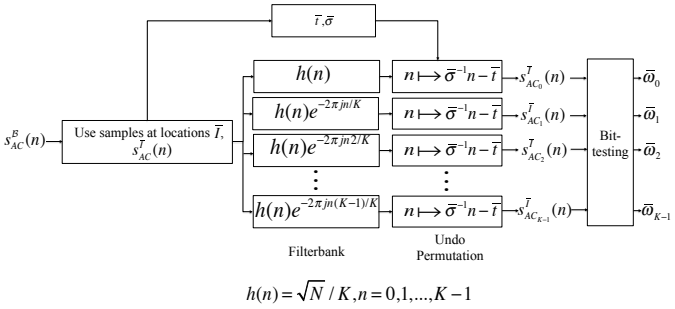

Fig. 3: A block diagram for Identification.

The SFT algorithm proceeds in an iterative fashion. First, the spatial frequencies i.e., $\omega_m = \frac{2f_c v_y y_m}{cR \cdot \text{PRF}}$ in (8c), are identified and their coefficients are estimated. Then, an approximation of the signal is constructed, and is subsequently subtracted from the observed processed signal. The same process is repeated for the residual signal to improve the estimation performance.

The SFT utilizes a set of pseudo-randomly selected points. With knowledge of odd numbers $\bar{\sigma}$, $\hat{\sigma}$ chosen from $\{1, 3, ..., N-1\}$ and integers $\bar{t}$, $\hat{t}$ chosen from $\{0, 1, ..., N-1\}$, the locations of the azimuth undersampled data used in identification and estimation denoted as $\bar{I}$ and $\hat{I}$, respectively, are given by

$$\bar{I} = \cup_{k=0}^{K-1}(\bar{t} + \bar{\sigma}(k-1) + I_0) \mod N, \tag{11}$$

$$\hat{I} = \cup_{k=0}^{K-1}(\hat{t} + \hat{\sigma}(k-1)) \mod N, \tag{12}$$

where $I_0 = \{0, 2^b\}$, $b = 0, 1, ..., \log_2 N/2$ and $\mathcal{B} = \bar{I} \cup \hat{I}$. The need of I_0 comes from the bit-testing procedure which will be explained detailedly in the following.

Fig. 3 shows a block diagram for the identification process [9]. To identify the spatial frequencies, the sampled signal at the locations $\bar{I}$, $s^{\bar{I}}_{AC}(n)$, is filtered by a box-car filter bank $h_k(n) = h(n)e^{-2\pi jnk/K}, k = 0, 1, ..., K-1$ with $h(n) = \sqrt{N}/K, n = 0, 1, ..., K-1$ containing $K = \lfloor uQ \rfloor$ frequency bins, where u is a small positive number and $u > 1$. The kth signal after the filter bank can then expressed as

$$\bar{s}^{\bar{I}}_{AC_k}(n) = \frac{\sqrt{N}}{K}\sum_{i=0}^{K-1} h(i)s^{\bar{I}}_{AC}(n - \bar{t} - \bar{\sigma}i)e^{-2\pi jik/K} \tag{13}$$

At a fixed point $n \in \{0, 1, ..., \log_2 N/2\}$ the values of $\bar{s}^{\bar{I}}_{AC_0}(n)$,...,$\bar{s}^{\bar{I}}_{AC_{K-1}}(n)$ can be calculated by the K-point FFT of the product of the sampled input signal with the filter. Since the sampling scheme leads to permutation of the spectrum of the azimuth signal, undo permutation as shown in Fig. 3 is applied to revert the locations of the spatial frequencies. Because there are only a few spatial frequencies, and due to the spectrum permutation, each bin $\{s^{\bar{I}}_{AC_k}(n), k = 0, 1, ..., K-1\}$ will probably contain a single significant frequency $\{\bar{\omega}_k, k = 0, 1, ..., K-1\}$. The frequency in each filter output can then

be identified via a process called bit-testing, as described in [8].

The estimation step provides the approximation of target coefficients corresponding to spatial frequencies identified in the previous step. If we aim to estimate the coefficient of a significant frequency ω, first, we demodulate the signal $s^{\mathcal{B}}_{AC}(n)$ by ω. The corresponding coefficient becomes the DC component of the demodulated signal. Then the sampled demodulated signal at the locations $\hat{I}$ is passed through a box-car low pass filter $h(n)$ to retain the zero frequency while attenuating the rest of the spatial frequencies. Afterward, the coefficient of the zero frequency is estimated as the mean of the first K samples of the filtered signal.

C. Discussion

Based on predefined values for N, K, $\bar{\sigma}, \bar{t}, \hat{\sigma}$ and $\hat{t}$, the set of indices for the range and azimuth sampling can be precomputed based on (11) and (12). Therefore, only samples at locations given by (11) and (12) enter the block diagram of Fig. 2. The range dechirp is performed on the undersampled data.

The number of azimuth samples needed in the above process based on (11) and (12) is $O(K \log_2 N)$ [8], which is much smaller than the number of azimuth Nyquist sampling points N. The same method can also be applied to the range compression. The number of range samples needed by the SFT-RD algorithm is $O(K \log_2 N_t)$ which is much smaller than the number of range Nyquist sampling points N_t. The computational complexity for the proposed method is $O(K \log_2 K)$ which is also much smaller than that of the RD algorithm $O(N \log_2 N)$ in azimuth direction and $O(N_t \log_2 N_t)$ in range direction.

IV. Experimental Results

In this section, we demonstrate the performance of the proposed SFT-RD imaging algorithm on synthetic SAR data and compare it with the classical RD imaging algorithm.

We set the speed of light and carrier frequency be $c = 3 \times 10^8$ and $f_c = 10^9$ Hz repectively. The radar at the initial position $\mathbf{p}_r(0) = [10000\sqrt{2}, 0, 10000\sqrt{2}]$ (m) moves at the speed of $\mathbf{v} = [0, 100, 0]$ m/s. The aperture time in the azimuth direction is $T_n = 0.5$ seconds with the pulse repetition frequency PRF $= 1024$. In addition, the pulse duration in range direction is $T_c = 5 \times 10^{-6}$ seconds with the bandwidth of the chirp signal $B = 2.048 \times 10^8$ Hz and sampling frequency in fast-time $F_{sr} = B$.

A single point target is simulated in the first example. The contour view of the imaging results using RD with full data and SFT-based RD with undersampled data are shown in Fig. 4a, Fig. 4d respectively. The SFT-based RD used only 10% of the data used by the FFT-based RD. From Fig. 4, it can be clearly observed that the point scatter using the SFT-based RD algorithm can be as well focused as the RD algorithm, which suggests that the SFT-based RD algorithm has the same resolution as the RD algorithm.

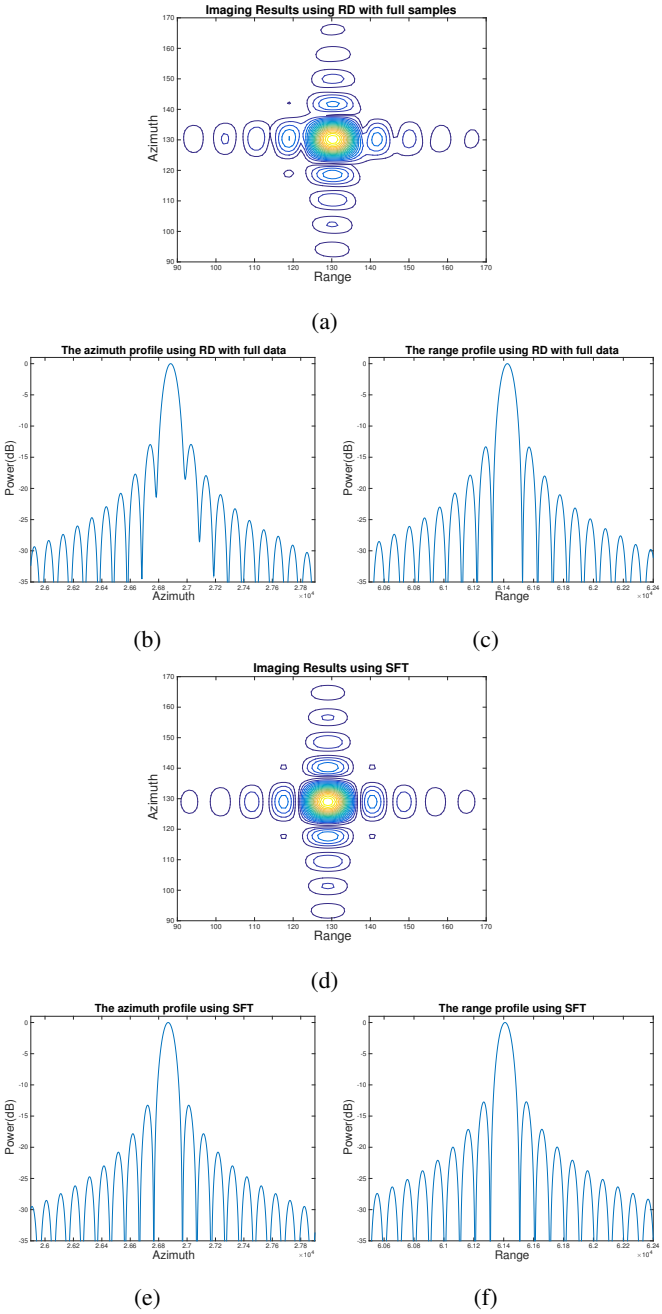

Fig. 4: (a) and (d) show contour representations of the imaging results using RD with full data and STF based RD with undersampled data respectively. (b) and (c) show the range and azimuth profiles respectively for the simulated point target along the axis for (a). (e) and (f) show the range and azimuth profiles respectively for the simulated point target along the axis for (c).

Twelve point targets are generated in the second example with randomly assigned unit power complex magnitude. Fig. 5a is the simulated raw data while Fig.5b shows the undersampled data used in the SFT-based RD. Fig. 5c illustrates the reconstruction of the twelve point targets with the full

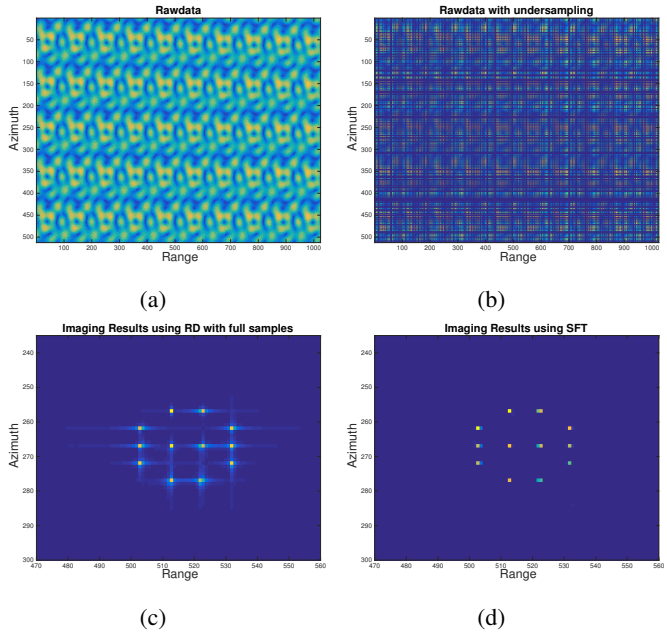

Fig. 5: Twelve point targets: (a) simulated full data (b) simulated data with undersampling (c) imaging results using RD with full samples (d) STF based RD imaging results with undersampled data.

data using RD and Fig. 5d shows the reconstruction of point targets with undersampled data (25% is used) using the SFT based RD algorithm. It is obvious that our proposed method produces the same resolution as the RD algorithm while using much fewer data.

V. Conclusion

In this paper, we proposed a SFT based RD algorithm for SAR imaging in a side-look spotlight mode. Our proposed method enables the SAR imaging to maintain the same resolution as the RD algorithm with computational complexity $O(K \log_2 K)$ while only employing $O(K \log_2 N_t)$ and $O(K \log_2 N)$ samples in range and azimuth direction respectively. The proposed method significantly reduces the burden brought by the imaging operations with a large amount of data.

Acknowledgment

The authors would like to thank Dr. Vishal Patel for his valuable suggestions.

References

[1] Cumming, Ian G., and Frank Hay-chee Wong, "Digital processing of synthetic aperture radar data: algorithms and implementation," Artech house, 2005.

[2] Carrara, Walter G., Ron S. Goodman, and Ronald M. Majewski,"Spotlight synthetic aperture radar- Signal processing algorithms," Norwood, MA: Artech House, 1995.

[3] Donoho, David L. , "Compressed sensing," Information Theory, IEEE Transactions on 52.4, pp. 1289-1306, 2006.

[4] Patel, Vishal M., Glenn R. Easley, Dennis M. Healy Jr, and Rama Chellappa,"Compressed synthetic aperture radar," Selected Topics in Signal Processing, IEEE Journal of 4, no. 2, pp. 244-254, 2010.

[5] Bu, Hongxia, Ran Tao, Xia Bai, and Juan Zhao,"A novel SAR imaging algorithm based on compressed sensing," Geoscience and Remote Sensing Letters, IEEE 12, no. 5, pp. 1003-1007, 2015.

[6] Wen, Hong, and Mao Shiyi,"Chirp and dechirp technique in spotlight mode SAR imaging," Signal Processing, 3rd International Conference on. Vol. 1. IEEE, 1996.

[7] A. Gilbert, P. Indyk, M. Iwen and S. Ludwig, "Recent Developments in the Sparse Fourier Transform: A compressed Fourier transform for big data," IEEE Signal Processing Magazine, vol. 31, no. 5, pp. 91-100, 2014.

[8] A. Gilbert, S. Muthukrishman and M. Strauss, "Improved time bounds for near-optimal sparse Fourier representations," International Society for Optics and Photonics, pp. 59141A-59141A, 2005.

[9] A. Gilbert, M. Strauss and J. Tropp, "A tutorial on fast Fourier sampling," IEEE Signal processing magazine, vol. 25, no. 2, pp. 57-66, 2008.

[10] Xiaqing Yang, Bo Li, and Athina P. Petropulu, "Colocated MIMO radars using the Sparse Fourier Transform," Applied Computational Electromagnetics (ACES), 2015 31st International Review of Progress in. IEEE, 2015.

[11] Y. Yu, A. P. Petropulu, and H. V. Poor, "MIMO radar using compressive sampling," IEEE Journal of Selected Topics in Signal Processing, vol. 4,no. 1, pp. 146-163, 2010.